geosciences

MDPI

Article

Gas Permeability Behavior in Frozen Sand Controlled by Formation and Dissociation of Pore Gas Hydrates

Evgeny Chuvilin *, Maksim Zhmaev and Sergey Grebenkin

Skolkovo Innovation Center, Skolkovo Institute of Science and Technology, 30. Build. 1, Bolshoi Boulevard, 121205 Moscow, Russia

* Correspondence: e.chuvilin@skoltech.ru

Abstract: Formation and dissociation of pore gas hydrates in permafrost can change its properties, including fluid flow capacity. Permeability is one of the most significant parameters in the study of hydrate-containing rocks, especially in the case of gas burial or extraction. Gas permeability variations in frozen sand partially saturated with CO_2 or CH_4 hydrates are studied experimentally at a constant negative temperature of −5 °C, as well as during freezing–thawing cycles. The gas permeability behavior is controlled by the formation and dissociation of pore gas hydrates in frozen sand samples. The samples with an initial ice saturation of 40 to 60% become at least half as permeable, as 40% of pore ice converts to hydrate. The dissociation process of accumulated hydrates was modeled by both depressurizing methane or CO_2 to atmospheric pressure and by stepwise injection of gaseous nitrogen up to 3 MPa into a frozen sample. In sand samples, with a decrease in gas pressure and without subsequent injection of nitrogen, a decrease in pore hydrate dissociation due to self-preservation was noted, which is reflected by a deceleration of gas permeability. Nitrogen injection did not lead to a decrease in the rate of dissociation in the frozen hydrate-containing sample, respectively, as there was no decrease in the rate of gas permeability.

Keywords: frozen sand; gas permeability; methane; carbon dioxide; formation, dissociation and self-preservation of pore gas hydrates

Citation: Chuvilin, E.; Zhmaev, M.; Grebenkin, S. Gas Permeability Behavior in Frozen Sand Controlled by Formation and Dissociation of Pore Gas Hydrates. *Geosciences* **2022**, *12*, 321. https://doi.org/10.3390/geosciences12090321

Academic Editors: Umberta Tinivella and Jesus Martinez-Frias

Received: 5 August 2022
Accepted: 23 August 2022
Published: 28 August 2022

1. Introduction

Natural gasses such as methane can exist in the form of hydrates, which constitute rich unconventional resources of hydrocarbons. Gas hydrates are crystalline clathrate compounds formed out of water molecules and low-molecular gas under certain pressures and temperatures [1–4]. Large amounts of greenhouse CO_2 are sequestered in gas hydrates in marine bottom sediments and permafrost within the shallow lithosphere, where the conditions are favorable for their formation and stability [5–8]. Carbon dioxide buried in hydrate form is highly concentrated; each cubic meter of pore CO_2 hydrate can store about 120 to 162 cubic meters of gas, even if the saturation is incomplete [9].

The processes of gas hydrate formation and dissociation have bearing on the porosity and permeability of hydrate-bearing sediments, and thus on engineering solutions for gas production from hydrate reservoirs potentially occurring in the Arctic gas fields. Gas hydrate formation induced by the operation of wells in permafrost may decrease permeability and the related fluid flow capacity and rates [10]. Under pressure and temperature changes, pore gas hydrates can dissociate into water and greenhouse gas while the latter is released into the atmosphere.

The behavior of permeability is also controlled by changes in the pore space of permafrost associated with phase transitions of pore moisture [11–14]. Pore moisture in permafrost can include liquid water, ice, gas, or gas hydrate, depending on rock composition, pressure, and temperature; e.g., thawing of permafrost increases the amount of free unfrozen water. Gas permeability can be estimated experimentally in frozen natural core

samples or laboratory model samples, under user-specified *PT* conditions that maintain the stability of pore ice and gas hydrate and affect phase changes of pore moisture.

The first experimental data on gas permeability of sand containing different percentages of pore ice and gas hydrates were obtained in the 1970s [15–18]. The interest to the permeability of ice- and hydrate-bearing sediments rekindled in the 2000s in relevance to methane production from hydrate-bearing reservoirs, including permafrost, and to emission of greenhouse gases in the Arctic.

Water permeability measured in core samples from the Mallik Methane Hydrate Site in Canada [19] showed an increase from ~2 mD before experiments to 17 mD after dissociation of pore hydrates. Experiments on the permeability of sediments from the northern slope of Alaska (Elbert Mt) to water and gas [20,21] allowed for tracing of permeability variations as a function of hydrate saturation; relative permeability decreased from 0.68 to 0.07 u.f. as the saturation increased from 1.5 to 36% [20]. Other experiments focused on the behavior of permeability depending on porosity and the presence of pore gas hydrates [21]). They revealed that permeability became about ten times higher upon a 4% porosity increase and up to three orders of magnitude (or more) lower upon saturation of sediments with gas hydrates [21].

In recent years, permeability of hydrate-bearing sediments has been studied in relation to their mechanical properties [22–25]. However, these studies were conducted at temperatures above 0 °C, i.e., for unfrozen rocks.

In addition to laboratory experiments, permeability in hydrate-saturated rocks at above-freezing temperatures was calculated theoretically and simulated numerically [12,26–32], but correlations between laboratory and modeling data have been insufficient for determining universal relationships.

Experimental investigation on the permeability behavior during the formation and dissociation of pore gas hydrates in ice-rich permafrost at phase transitions of pore moisture (ice–liquid, water–gas hydrates) under climate-induced changes of pressure and temperature are of special importance in Arctic studies. Previously, we [33–35] observed significant permeability reduction in hydrate-bearing sand and silty sand exposed to freezing temperatures, due to the conversion of residual liquid pore water to ice and additional hydrate formation. On the other hand, hydrates can form in thawing hydrate-bearing samples at low positive temperatures and above-equilibrium gas pressures. Gas permeability of frozen hydrate-bearing sediments can also change upon temperature- and pressure-driven phase transitions, or upon injection of gases that inhibit hydrate formation [35,36].

However, these issues have not been experimentally studied to a sufficient extent. With the exception of the Skoltech scientific group, research on the gas permeability of frozen hydrate-containing rocks at low temperatures is practically nonexistent. To bridge the gap, special experiments have been performed to estimate gas permeability variations in frozen hydrate-bearing sand associated with formation and dissociation of pore gas hydrates, at a below-equilibrium pressure and under the effect of inhibitor gas injected into sediments at negative temperatures.

2. Methods

The effects of water–ice–hydrate transitions within pore moisture and gas transport on the gas permeability behavior of sediments were studied using a specially designed method simulating the Arctic conditions [35]. The method consists of gas flushing in a system designed by *EkoGeosProm* LLC (Figure 1) that can provide *PT* ranges of –15 to +30 °C and up to 10 MPa. The equipment was located inside a climate chamber, which allows for maintaining of the temperature with an accuracy of 0.1 C. The confining stress was set using a hydraulic pump, which increases the oil pressure in the core holder around the rubber sleeve with the sample. The system can handle soil samples 30 mm in diameter and 30–50 mm long, either core samples or pre-compacted porous soil. Linear non-stationary gas filtration through a soil sample was used in this system. The accuracy of gas permeability measurements, according to calibration on model samples, is no lower than 10% [37].

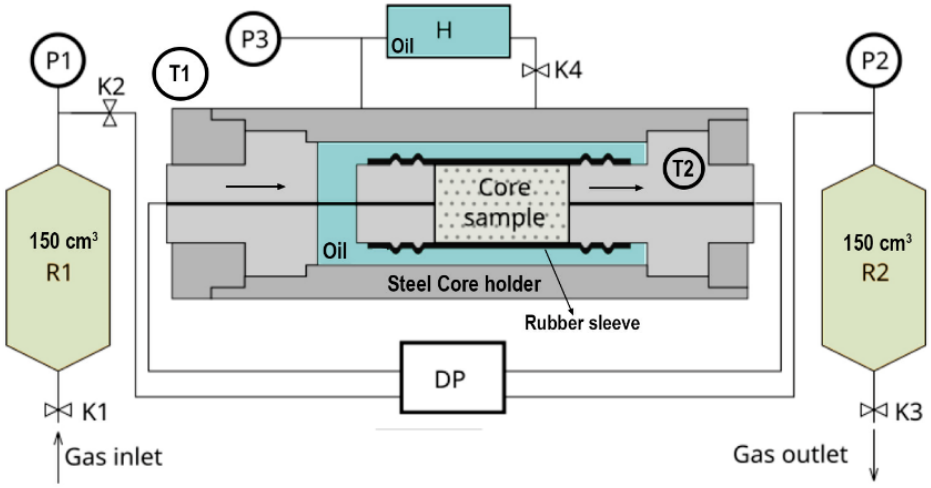

Figure 1. System for gas permeability measurements: K1 − K3 = diaphragm valves with pneumatic control, K4 = ball valve with pneumatic control, R1 − R2 = reservoirs with gas, P1 − P3 = pressure sensors, DP = differential pressure sensor, T1 − T2 = temperature sensors, H = hydraulic pump for confining stress.

The following technique was used to prepare the samples. Air-dry sand cooled to negative temperatures was mixed in a cold room (−5 °C) with a known mass of crushed ice. Crushed ice (ice particles less than 1 mm) was used in the preparation of samples to obtain a uniform distribution of moisture. A moisture content of 10% was set for the studied samples. Then, this sediment was kept at room temperature (about +20 °C) and thawed. This thawed sediment was then placed in a rubber sleeve (3–4 cm high and 3 cm in diameter) and compacted layer by layer. Then, the samples were put into a pressure vessel inside a metal container, compressed to 6 MPa, frozen for 24 h at −5 °C, after which the system vacuumed them before injection of hydrate-forming gases (point 1 in Figure 2). Depending on the compaction of the samples, the ice's degree of saturation of the pore space ranged from 31 to 55% before the start of gas injection.

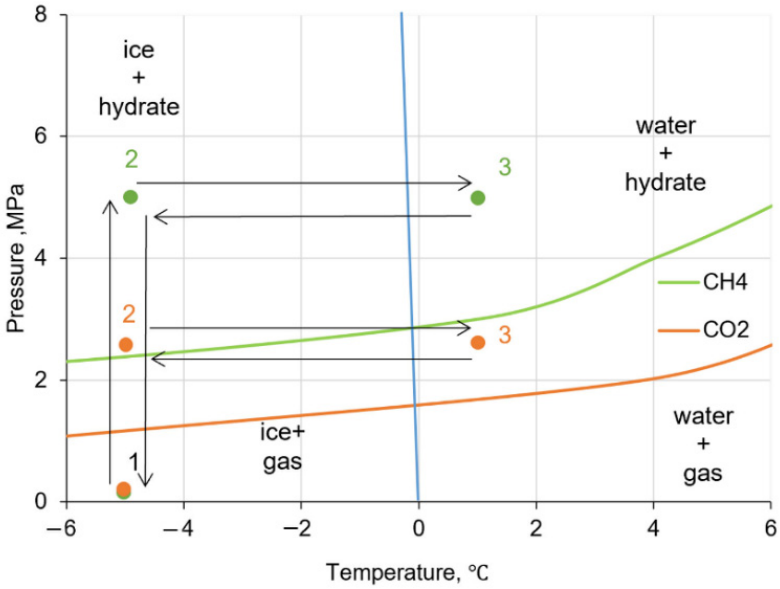

Figure 2. Phase diagrams for CH_4 and CO_2 hydrates and *PT* conditions of experiments: green and orange points refer to runs with CH_4- and CO_2-saturated sand samples, respectively. Arrows show direction of pressure and temperature changes.

Hydrate-forming gas (CO_2 or CH_4) was injected stepwise, up to 5 MPa for CH_4 (green point 2 in Figure 2) and 2.5 MPa for CO_2 (orange point 2 in Figure 2). During all experiments, the pressure difference between the ends of the frozen sample at injection did not exceed 0.5 MPa. The hydrate saturation occurred at a constant temperature of −5 °C, with periodic gas flushing of samples in order to monitor their effective gas permeability. In some runs, the samples were heated to +1 °C after hydrate saturation (point 3 in Figure 2), and underwent additional hydrate formation as the released unfrozen water converted to hydrate.

After hydrate saturation had completed, the samples were depressurized to 0.1 MPa, or below equilibrium (arrow 2 → 1 in Figure 2), whereby gas hydrates dissociated at a temperature of −5 °C. Gas hydrate dissociation was additionally stimulated in some samples by injection of nitrogen after pressure release. At the end of the tests, the samples were taken out of the pressure vessel and measured for final moisture contents, weight, and size (length and diameter). The temperature and pressure in the vessel were monitored continuously during the experiment.

The pressure–volume–temperature (PVT) analysis was applied to infer different parameters of the samples from pressure and temperature changes: effective gas permeability (K) and relative gas permeability (K_r) (defined as the ratio of the effective permeability of a hydrate-rich sample to the permeability of a sample without hydrate); consumption of hydrate-forming gas (Δm_G); weight of pore gas hydrate (M_h); hydrate contents (H); saturation with ice (S_i), water (S_w), and hydrate (S_h); as well as hydrate coefficient (K_h), which refers to the fraction of pore water converted to hydrate [11,35,38].

Consumption of methane or carbon dioxide (Δm_G, g) was calculated as

$$\Delta m_g = \frac{\Delta P_i \cdot V_c \cdot M}{R \cdot T_i \cdot z} \quad (1)$$

where ΔP_i—pressure at a point in time τ_i (MPa), V_c—reduced volume of the pressure cell (cm^3), M—methane or carbon dioxide molar mass (g/mol), R—universal gas constant (N·m/K·mol), T_i temperature at a point in time τ_i (K), and z—compressibility factor, which was calculated by equation of state.

Based on the consumption of methane or carbon dioxide during hydrate formation and on the chemical formula of methane hydrate—$CH_4 \cdot 5.9H_2O$, carbon dioxide—$CO_2 \cdot 6.1H_2O$, the weight of pore gas hydrate (M_h, g) was calculated assuming a hydrate number of 5.9 for CH_4 and 6.1 for CO_2 as

$$M_h(CH_4) = \Delta m_g \cdot 5.9 \quad (2)$$

$$M_h(CO_2) = \Delta m_g \cdot 6.1 \quad (3)$$

The volume content of hydrate (H, %) at each point in time was found as

$$H = \frac{M_h \cdot p}{M_s \cdot p_h} \cdot 100 = \frac{V_h}{V_v} \cdot 100 \quad (4)$$

where Ms is the weight of the soil sample (g), ρ is the sample density (g/cm^3), ρ_h is the crystallographic density of an empty square lattice (without gas molecules by analogy with the pure ice structure, g/cm^3), V_h is the volume of hydrate (cm^3), V_v is the volume of the voids created by the soil particles(cm^3).

Hydrate saturation, or the percentage of pore space filled with hydrate (S_h, u.f.), is inferred from the volume content of hydrate as

$$S_h = \frac{H}{n} = \frac{V_h}{V_v} \quad (5)$$

where n is the sample porosity (u.f.) as

$$n = \frac{p_s - p_d}{p_s} = \frac{V_v}{V} \quad (6)$$

where ρ_s—solid particles density (g/cm^3), ρ_d—dry unit weight (g/cm^3), and V is the unit volume of soil (cm^3).

Ice saturation or percentage of pore space filled with ice (S_i, %) as

$$S_i = \frac{W \cdot p_d}{0.92 \cdot n} \cdot 100 \quad (7)$$

The fraction of water converted to hydrate or the hydrate coefficient (K_h, u.f.) is given by

$$K_h = \frac{W_h}{W} \quad (8)$$

where W_h is the percentage of water converted to hydrate (% of dry sample weight) calculated assuming a hydrate number of 5.9 for CH_4 and 6.1 for CO_2, and W is the total amount of moisture (initial water content, %).

The effective permeability (K) of samples in the pressure vessel was inferred from pressure drop in reservoirs with a known volume of gas by solving the differential equation of mass transfer through the sample under the pressure gradient

$$K = \frac{2\eta L V_1 p_1}{S p_{10}(p_1^2 - p_2^2)} \cdot \frac{p_{10} - p_{1k}}{p_1 t_1} \quad (9)$$

where η is the dynamic viscosity of the gas, Pa·s; L is the sample length, cm; S is the sample cross-sectional area, cm^2; V_1 is the reservoir volume, cm^3; p_1 is the pressure at sensor P1 (Figure 1) at the time t_1, MPa; p_2 is the pressure at sensor P2 at the time t_1, MPa; p_{10} is the pressure at sensor P1 at t_0 (start), MPa; p_{1k} is the pressure at sensor P1 at t_k (end), MPa; K is the gas permeability, mD.

Gas permeability was studied in quartz sand sampled from frozen Quaternary marine deposits (mQ_3) of the South Tambei gas condensate field in the Yamal Peninsula. The sand is light gray, homogeneous, and rounded; its mineralogy consists mostly of quartz (93.7%), with minor amounts of albite (5.1%) and orthoclase (1.2%). The properties of the sand are as follows: mainly (62.3%) 0.25–0.1 mm particle sizes (Table 1); 2.67 g/cm^3 air-dry density; 0.06% salinity; and 0.24 m^2/g specific surface area.

Table 1. Particle size distribution of sand samples.

Soil Type (ASTM D2487-17)	Particle Size (mm) Distribution, %						Mineralogy
	1–0.5	0.5–0.25	0.25–0.1	0.1–0.05	0.05–0.001	<0.001	
Fine sand with silt	0.2	29.1	62.3	2.4	5.8	1.2	>93% quartz

Experiments were performed on five quartz sand samples (S1 to S5) with 10–11% moisture contents at porosity 0.35–0.37 u.f. for S1–S3 and 0.46–0.48 u.f. for S4–S5 (Table 2).

Table 2. Properties of frozen sand samples prior to hydrate saturation.

Run	Moisture Content, %	Density, g/cm^3	Porosity, u.f.	Initial Ice Degree of Saturation (S_i,%)	Initial Gas Permeability, mD
S1	10	1.88	0.36	49.3	16.24
S2	10	1.95	0.35	53.7	17.95
S3	11	1.87	0.37	54.6	18.11
S4	10	1.52	0.48	30.6	18.76
S5	10	1.59	0.46	34.3	21.08

Ice saturation varied between samples, from 30.6% for S4 to 54.6% for S3. The initial gas permeability prior to hydrate saturation ranged from 16.24 to 21.08 mD. Ice saturation (S_i) of each sample was calculated after compression and freezing, and the initial gas permeability was measured experimentally (Table 2). The permeability was the highest in sample S5 (21.08 mD), which had 34.3% ice saturation and 0.46 u.f. porosity, and was the lowest in S1 (16.24 mD) with higher ice saturation (50%).

3. Experimental Results & Discussion

3.1. Gas Permeability Behavior in Frozen Sand during Hydrate Formation

The five frozen sand samples, with initial gas permeability measured, were partially filled with hydrates of carbon dioxide (CO_2) for S1–S3, and methane (CH_4) for S4 and S5. First, hydrate formation in all samples occurred at a constant negative temperature of −5 °C (Table 3), for a period from two (S2) to ten (S5) days. As hydrate formation in S2 and S4 decelerated, the samples were heated to +1 °C, which led to thawing and reactivation of the hydrate formation process (Table 4). Then, sample S2 was frozen back to −5 °C in order to estimate the amount of additional gas hydrate that formed when the residual liquid pore water was converted to ice. Thus, the phase state of pore moisture was characterized for all samples, and gas permeability was constrained at each hydrate saturation step (Tables 3 and 4).

Table 3. Properties of frozen sand samples during hydrate formation at constant negative temperature (−5 °C).

Run	Time, h	K_h, u.f.	S_i, %	S_h, %	$S_i + S_h$, %	$K_{\text{eff av}}$, mD
S1	0	0	49.3	0	49.3	16.24
	24	0.27	31.65	21.69	53.34	11.27
	48	0.32	35.43	25.88	61.31	10.66
	72	0.46	29.19	36.92	66.11	6.42
S2	0	0	53.7	0	53.7	17.95
	24	0.26	40.36	24.37	64.73	12.47
	48	0.37	35.87	32.35	68.22	10.44
S3	0	0	54.6	0	54.6	18.11
	24	0.34	38.51	29.71	68.22	7.88
	48	0.43	34.21	37.41	71.62	6.44
	144	0.59	26.32	51.57	77.89	5.99
	168	0.64	23.52	56.59	80.11	5.47
S4	0	0	30.6	0	30.6	18.76
	72	0.29	22.63	12.01	34.64	12.7
	168	0.42	18.99	17.40	36.39	9.23
S5	0	0	34.3	0	34.3	21.08
	96	0.38	22.92	17.53	40.45	12.59
	120	0.49	19.51	22.61	42.12	11.12
	192	0.54	17.73	25.25	42.98	10.77
	240	0.59	16.21	27.51	43.72	10.25

Table 4. Parameters of frozen hydrate-rich sand thawed and refrozen under the conditions of hydrate formation.

Run		K_h, u.f.	S_i (S_w), %	S_h, %	$S_i + S_h$, %	$K_{\text{eff av}}$, mD
S2	−5	0.37	35.87	32.35	68.22	10.44
	+1	0.48	30.72	41.52	72.24	10.17
	−5	0.61	24.26	52.97	77.23	8.92
S4	−5	0.42	18.99	17.40	36.39	9.23
	+1	0.51	16.68	26.8	43.48	1.60

The gas permeability of the samples decreased as more moisture converted to hydrate (K_h), and the hydrate saturation (S_h) increased correspondingly (Figures 3 and 4; Tables 3 and 4).

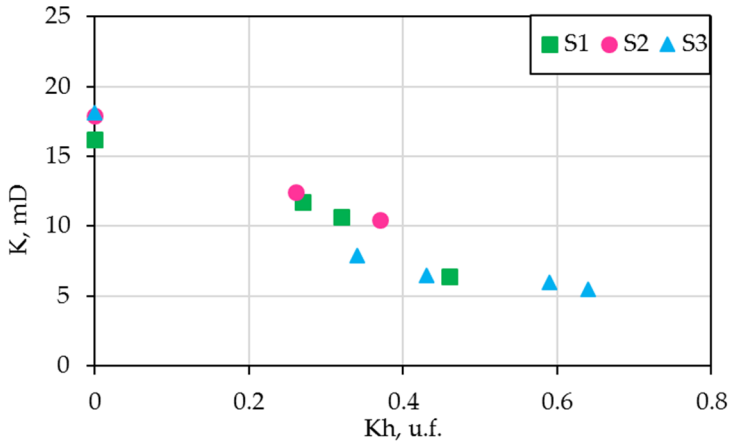

Figure 3. Effective gas permeability of frozen sand vs. CO_2 hydrate coefficient (K_h) at −5 °C.

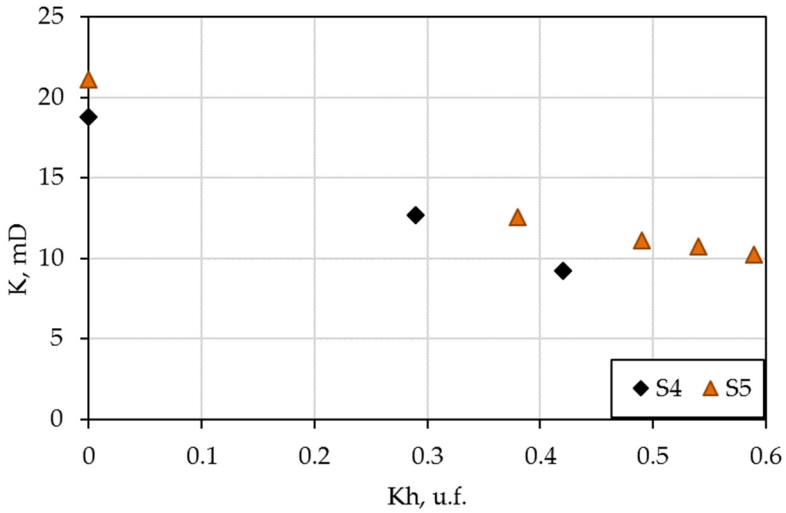

Figure 4. Effective gas permeability vs. hydrate coefficient for methane hydrate at −5 °C.

The gas permeability of S1 decreased from 16.24 mD to 11.27 mD as K_h grew to 0.27 u.f. Upon further conversion of pore ice to hydrate, up to K_h = 0.46 u.f., gas permeability decreased to 6.42 mD, or 2.5 times lower than the initial value. Hydrate formation in S2 (to K_h = 0.26 u.f.) at −5 °C led to 1.5-fold decrease of gas permeability. As the hydrate coefficient increased to 0.37 u.f., gas permeability reduced by an additional 16%. Heating of the sample to +1 °C led to K_h change from 0.37 to 0.48 u.f., while the permeability decreased only slightly from 10.44 to 10.17 mD and then to 8.92 mD when the sample was frozen back to −5 °C, i.e., it became almost twice as low as prior to hydrate saturation. Hydrate saturation of S3 occurred at negative temperature only (−5 °C). Gas permeability decreased from 18.11 mD to 7.88 mD as K_h grew to 0.34 u.f. and further to 5.47 mD at K_h = 0.64 u.f., or three times lower than the initial value (Figure 3).

The formation of methane hydrates in the frozen sediments at −5 °C likewise led to a gas permeability decrease (Table 3; Figure 4). As 42% of pore ice in S4 converted to hydrate, its permeability changed from 18.76 mD to 9.23 mD, or became almost twice as low as prior to hydrate formation. Thawing of the sample at +1 °C led to a permeability decrease to 1.60 mD (five times lower than the initial value), due to additional hydrate formation upon thawing as well as to uneven distribution of locally migrating moisture [35]. Formation of methane hydrate in S5 at −5 °C was accompanied by K_h increase to 0.59 u.f. and the ensuing gas permeability decrease from 21.08 mD to 10.25 mD.

Calculations predict that the total ice + hydrate saturation during conversion of pore ice to hydrate increases on account of the ~15% difference in specific volume between

ice and gas hydrate [34,35]. As a result, the pore space shrinks (1 − (Si + Sh)), and the permeability reduces correspondingly (Figure 5).

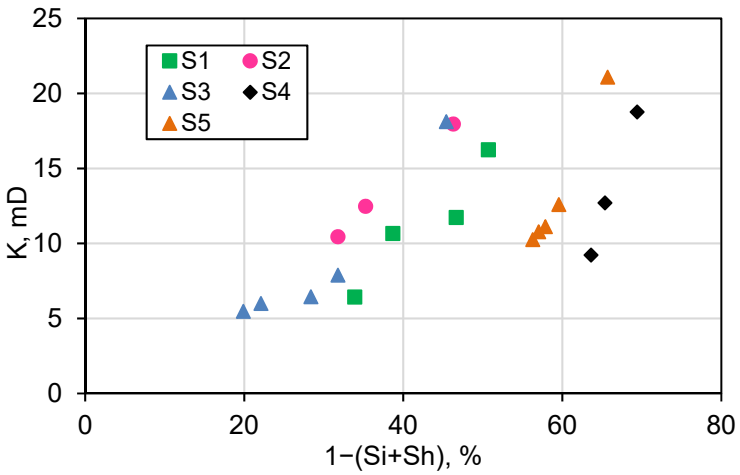

Figure 5. Gas permeability of frozen sand vs. relative pore space volume (1 − (Si + Sh)) during hydrate formation at −5 °C.

The pore space reduction in samples S1–S3 with relatively low porosity (0.35–0.37 u.f.) reached a magnitude of 1.5–2.5, as 40–60% of pore ice converted to CO_2 hydrate, which led to a 3.0 or 3.5-fold decrease in gas permeability.

Samples S4–S5, with higher porosities of 0.46–0.48 u.f., in which pore ice converted to methane hydrate, had lower initial ice saturations, greater pore space volumes, and accordingly higher permeability in the beginning of the experiments. However, hydrate formation at a constant temperature of −5 °C provided a two-fold decrease of gas permeability while the pore space became 5–10% smaller.

Experiments that tested relative gas permeability (K_r) variations as a function of hydrate coefficient (K_h) in sand undergoing hydrate formation revealed a K_r decrease to 0.5–0.3 u.f., as 40–60% of pore ice converted to gas hydrate (Figure 6).

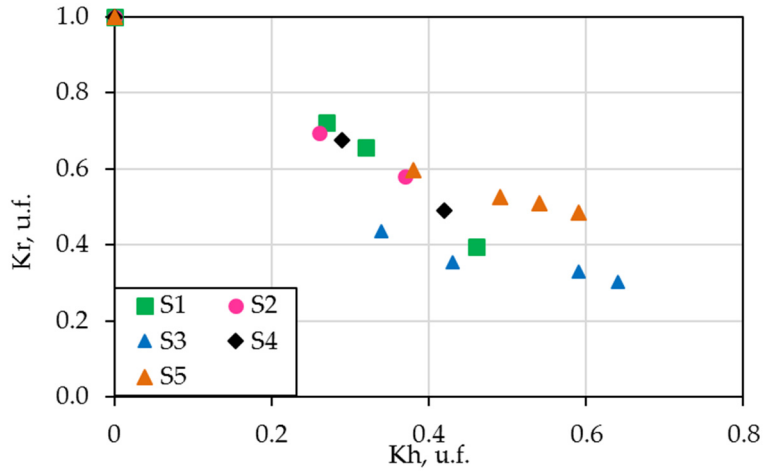

Figure 6. Relative gas permeability (K_r) as a function of hydrate coefficient.

3.2. Gas Permeability of Frozen Hydrate-Bearing Sand under Conditions of Hydrate Dissociation

The effect of pore hydrate dissociation on the permeability of frozen hydrate-bearing sand was studied at −5 °C and pressures of 0.1 MPa and 3.0 MPa.

Pressure increase to ~3 MPa was provided by injection of nitrogen, which inhibits hydrate formation, into the vessel with samples. Nitrogen was injected into samples S1–S3 immediately after the carbon dioxide pressure was reduced to 0.1 MPa. After reducing the

methane pressure in the S4 sample to 0.1 MPa, nitrogen was injected into the sample after three days.

Dissociation of pore CO_2 hydrate in samples S1 to S3, which were periodically flushed with gas to monitor effective gas permeability, continued from six to eight days (Figure 7). It was induced by destabilization as CO_2 was replaced by N_2, which cannot form hydrates at this pressure and temperature, but can displace CO_2 from the hydrate structure.

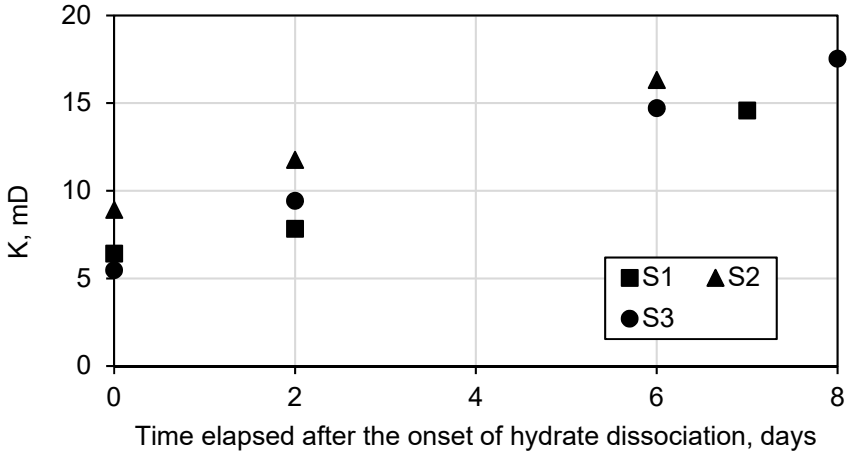

Figure 7. Gas permeability of frozen sand saturated with CO_2 hydrate at below-equilibrium pressure and nitrogen injection to 3 MPa, at −5 °C.

Gas permeability in S1 increased from 6.42 mD to 7.82 mD in two days after nitrogen injection, and reached 14.57 mD (10.3% below the initial value prior to hydrate saturation) after seven days of dissociation. This difference is due to the possibility of structural and textural transformations in the soil sample during the formation of hydrate in the pore space and its dissociation, which can lead to the narrowing of some pores and changes in filtration channels. Dissociation of CO_2 hydrate in S2 after nitrogen injection led to a permeability increase from 8.92 mD to 16.31 mD (9.1% below the initial permeability) in six days. Gas permeability in S3 likewise grew almost linearly with time after N_2 injection, from 5.47 mD to 17.53 mD, in eight days (only 3.2% lower than prior to hydrate saturation).

In the case of S4, pore methane hydrate dissociated before the injection of nitrogen, at −5 °C and 0.1 MPa. At that point, the dissociation delayed being impeded by an ice coat on the surface of hydrate due to its self-preservation [39,40]. That period was limited to three days, and then the dissociation resumed when cold nitrogen was injected into the sample. In general, dissociation of pore CH_4 hydrate in S4 at that stage was similar to the respective, not-yet-decelerated process for CO_2 in S1–S3, in the presence of nitrogen.

The dissociation of pore methane hydrate at 3 MPa after nitrogen injection was compared to that at 0.1 MPa with reference to earlier experimental data [35,36] for a similar sand sample (TS2) which had higher saturation in ice and hydrate (68.7%). The gas permeability of TS2 before dissociation of the pore gas hydrate was as low as 0.03 mD, but increased to 0.5 mD for the first six hours of dissociation after the pressure dropped to 0.1 MPa at −5 °C, and increased further to 1.0 mD 24 h after the onset of the experiment. Then, the dissociation process slowed down; gas permeability became only slightly higher (1.1 mD) in the following 36 h (Figure 8).

The gas permeability of sample S4 increased from 1.60 mD to 3.82 mD in three days after the methane pressure decreased to 0.1 MPa (Figure 8). Judging by our previous results, the increase was apparently fastest in the first days: to 6.53 mD (1.7 times the initial value) in two days after nitrogen injection, and then to 15.78 mD in the following three days, i.e., the nitrogen injection accelerated the dissociation process. Meanwhile, the final permeability was 16% lower than prior to hydrate saturation. Thus, pore gas hydrate in S4 did not undergo self-preservation upon depressurization, unlike TS2. On

the contrary, dissociation of residual pore hydrate became more active after N_2 injection to 3 MPa, whereby the sample became more permeable to gas.

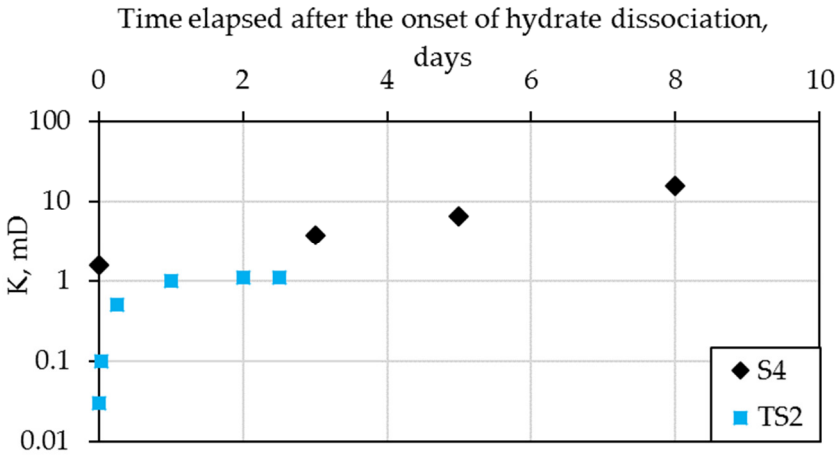

Figure 8. Gas permeability of frozen hydrate-bearing sand S4 and TS2 at non-equilibrium pressure and −5 °C. Hydrate dissociation at 0.1 MPa (up to 3 days) and 3 MPa, after nitrogen injection to 3 MPa (after 3 days).

3.3. Discussion of the Results

The analysis of data on changes in the gas permeability of frozen gas-saturated sand under conditions of hydrate formation, ice-water-hydrate phase transitions and dissociation of pore hydrates, which were obtained during the experiments, allows us to present the main processes that occur in the porous space of the studied samples in the following way (Figure 9). At the first stage, when a frozen sandy sample with a low degree of pore filling with ice is saturated with hydrate-forming gas to a pressure above equilibrium, the transition of pore ice into hydrate occurs (Figure 9b). This process is generally damped in time, which is due to the kinetics of hydrate formation associated with the deterioration of the permeation of the hydrate-forming gas to the front of the ice-hydrate phase transition [41]. Considering that when ice transforms into hydrate the specific volume increases by 9%, there is a regular decrease in gas permeability over time, while the rate of its decrease over time declines [35].

In order to activate the process of hydrate formation in the pore space of frozen sandy samples, in some experiments, an increase in temperature above 0 °C was used while maintaining gas pressure above equilibrium. The melting of pore ice that did not turn into hydrate under these conditions caused additional hydrate formation (Figure 9c). This is due to structural and textural changes which lead to the appearance of new gas–water contacts in the pore space of the soil, as well as the possible migration of pore moisture in the sand sample to the front of hydrate formation. This was reflected in a significant decrease in gas permeability. Further, upon repeated freezing of the sample to a temperature of −5 °C, additional hydrate formation was also observed, caused by the development of physical and mechanical processes during freezing [42]. At this stage, a decrease in gas permeability in the studied samples was also noted, caused by an increase in the total degree of pore filling with hydrate and ice (Figure 9d).

At the next stage, when the pressure of the hydrate-forming gas is reduced to an atmospheric level (0.1 MPa), in a frozen hydrate-containing sample at a fixed negative temperature of −5 °C, surface dissociation of the pore hydrate occurs with the formation of supercooled water and gas. This causes an increase in the gas permeability of the sand sample. Being in a nonequilibrium state, supercooled water freezes on the surface of hydrate particles with the formation of an ice crust, which prevents further decomposition of gas hydrate. As a result, the growth of gas permeability stops (Figure 9e). When nitrogen is injected into a frozen hydrate-containing sample under non-equilibrium conditions, the decay of pore hydrate dissociation is not observed, i.e., the effect of its self-preservation is

reduced. Apparently, when nitrogen is injected, a looser ice crust is formed, which does not prevent the active dissociation of the pore hydrate. This is reflected in the continuous increase in the gas permeability of the sample over time (Figure 9f).

The experimental features of changes in the gas permeability of frozen gas-saturated sand rocks under conditions of pore ice–water–hydrate phase transitions expand our knowledge of how the filtration properties of gas-saturated rocks in the cryolithozone transformed during their evolution.

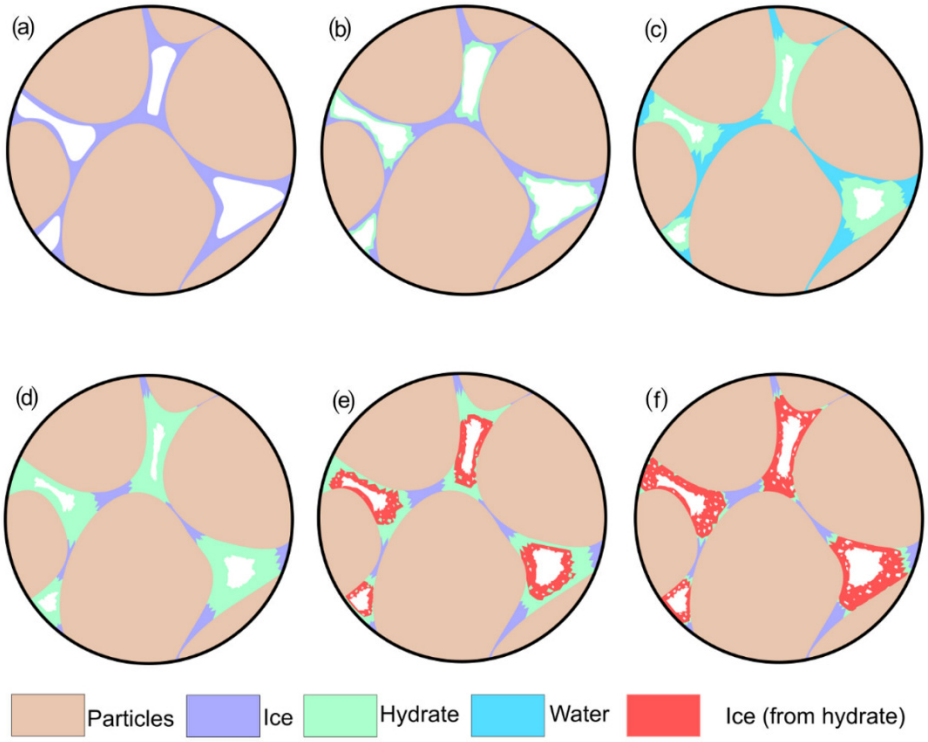

Figure 9. Pore space changes in gas-saturated sediments exposed to hydrate formation at t < 0 °C, thawing and freezing, and hydrate dissociation at t < 0 °C. Stages: (**a**) initial (before hydrate formation), (**b**) hydrate formation at t < 0 °C, (**c**) thawing, (**d**) freezing, (**e**) self-preservation of pore hydrate at p = 0.1 MPa, (**f**) hydrate dissociation at N2 atmosphere, p = 3 MPa.

4. Conclusions

The gas permeability of sand samples saturated with CO_2 and CH_4 hydrates, in a laboratory at a constant negative temperature of −5 °C, as well as in thawing–freezing cycles from +1 °C to −5 °C, is controlled both by ice saturation and by the kinetics of the transition of pore ice into hydrate and the fraction of its transition.

The permeability of frozen samples with 40–60% initial ice saturation becomes at least twice low, as 40% of ice converts to hydrate, both in the case of CO_2 and CH_4 hydrates, but further increases as the hydrate coefficient causes only a minor permeability decrease (Figures 3 and 4). Ice–water phase transitions during heating and cooling accelerate hydrate accumulation and decrease gas permeability as well.

It should be noted that a significant decrease (by up to five times or more) in the gas permeability of frozen hydrate-containing rocks occurs during their thawing under conditions of hydrate formation, when new gas–water contacts arise in the pore space, causing additional hydrate formation. Thus, an increase in the temperature of a frozen hydrate-containing sand sample from −5 °C to +1 °C led to gas permeability shifting from 9.23 mD to 1.60 mD, while K_h increased from 0.42 to 0.51 (Table 4).

A special study was carried out to investigate changes in the permeability of frozen hydrate-saturated sand rocks during dissociation, caused by reductions in the pressure of the hydrate-forming gas at a constant negative temperature of −5 °C to atmospheric

pressure, and with the injection of nitrogen gas acting as an inhibitor. It is noted that when the gas pressure in frozen hydrate-containing samples is reduced to an atmospheric level, there is a natural decrease in the dissociation of the pore hydrate over time, which is reflected by a deceleration in gas permeability.

However, when nitrogen is injected, there is no decrease in the dissociation of the pore hydrate over time and its self-preservation. Thus, in all samples saturated with CO_2 hydrates, a stable increase in gas permeability was observed after a stepwise injection of nitrogen into the samples up of to 3 MPa.

At the same time, during the observations (up to eight days), the permeability of the samples did not stabilize, in contrast to the change in permeability under conditions of self-preservation of porous hydrates at atmospheric pressure (0.1 MPa). Injection of nitrogen into a frozen sandy sample containing methane hydrates after the gas pressure was released, when self-preservation of the pore hydrate was observed, initiated dissociation of the pore hydrate, which was reflected in acceleration of gas permeability. This indicates the effect of nitrogen injection on the kinetics of pore hydrate dissociation. The gas permeability of samples at the end of these experiments was 3% to 16% lower than the initial value prior to hydrate formation, possibly due to the presence of a residual pore hydrate and to changes in the pore space upon phase transitions of the pore moisture.

The observed permeability variations can be referenced to create predictive models of the behavior of frozen hydrate-saturated reservoirs in the cryolithozone, and for developing technologies for the decomposition of relict gas hydrate accumulations.

Author Contributions: Conceptualization, experimental methodology, supervision, E.C.; experimental work, M.Z. and S.G.; processing and analysis, E.C. and M.Z.; writing, original draft preparation, E.C., M.Z. and S.G.; writing, review and editing, E.C., M.Z. and S.G. All authors have read and agreed to the published version of the manuscript.

Funding: The research was supported by the Russian Science Foundation (grants No. 21-77-10074 and 22-17-00112) and by the Tomsk State University Development Program (Priority 2030).

Data Availability Statement: Not Applicable.

Conflicts of Interest: The authors declare no conflict of interest.

References

1. Makogon, Y.F. *Hydrates of Natural Gases*; Nedra: Moscow, Russia, 1974; p. 208. (In Russian)
2. Istomin, V.A.; Yakushev, V.S. *Gas Hydrates in Nature*; Nedra: Moscow, Russia, 1992; p. 235. (In Russian)
3. Sloan, E.D. *Clathrates Hydrates of Natural Gas*, 2nd ed.; Marcel Dekker Inc.: New York, NY, USA, 1998; p. 757.
4. Max, M.D. *Natural Gas Hydrate in Oceanic and Permafrost Environments*; Kluwer Academic Publishers: Dordrecht, The Netherlands; London, UK, 2000; p. 414. ISBN 1384–6434.
5. Duchkov, A.D.; Sokolova, L.S.; Ayunov, D.E.; Permyakov, M.E. Assesment of potential of West Siberian permafrost for the carbon dioxide storage. *Earth's Cryosphere* **2009**, *23*, 62–68.
6. Chuvilin, E.; Guryeva, O. The role of hydrate formation processes in industrial CO_2 sequestration in permafrost area. In Proceedings of the 7th International Conference on Gas Hydrates (ICGH 2011), Edinburgh, UK, 17–21 July 2011.
7. Hassanpouryouzband, A.; Yang, J.; Tohidi, B.; Chuvilin, E.; Istomin, V.; Bukhanov, B. Geological CO_2 capture and storage with flue gas hydrate formation in frozen and unfrozen sediments: Method development, real time-scale kinetic characteristics, efficiency, and clathrate structural transition. *ACS Sustain. Chem. Eng.* **2019**, *7*, 5338–5345. [CrossRef]
8. Zheng, J.; Chong, Z.R.; Qureshi, F.; Linga, P. Carbon dioxide sequestration via gas hydrates: A potential pathway toward decarbonization. *Energy Fuels* **2020**, *34*, 10529–10546. [CrossRef]
9. Wright, J.F.; Cote, M.M.; Dallimore, S.R. Overview of regional opportunities for geological sequestration of CO_2 as gas hydrate in Canada. In Proceedings of the 6th International Conference on Gas Hydrates (ICGH 2008), Vancouver, BC, Canada, 6–10 July 2008.
10. Istomin, V.A.; Fedulov, D.M.; Minakov, I.I.; Kvon, V.G.; Burakova, S.V. Hydrates prevention in the bottom hole formation zone at high reservoir water salinity. In *Vesti Gazovoy Nauki: Problems of Operation of Gas, Gas Condensate and Oil and Gas Fields*; Gazprom VNIIGAZ: Moscow, Russia, 2013; Volume 4, pp. 15–21.
11. Chuvilin, E.; Bukhanov, B. Effect of hydrate accumulation conditions on thermal conductivity of gas-saturated soils. *Energy Fuels* **2017**, *31*, 5246–5254. [CrossRef]
12. Ren, X.; Guo, Z.; Ning, F.; Ma, S. Permeability of hydrate-bearing sediments. *Earth Sci. Rev.* **2020**, *202*, 103100. [CrossRef]

13. Waite, W.F.; Santamarina, J.C.; Cortes, D.D.; Dugan, B.; Espinoza, D.N.; Germaine, J.; Jang, J.; Jung, J.W.; Kneafsey, T.J.; Shin, H.; et al. Physical properties of hydrate-bearing sediments. *Rev. Geophys.* **2009**, *47*, RG4003. [CrossRef]
14. Yoneda, J.; Jin, Y.; Muraoka, M.; Oshima, M.; Suzuki, K.; Walker, M.; Otsuki, S.; Kumagai, K.; Collett, T.S.; Boswell, R.; et al. Multiple physical properties of gas hydrate-bearing sediments recovered from Alaska North Slope 2018 Hydrate-01 Stratigraphic Test Well. *Mar. Pet. Geol.* **2021**, *123*, 104748. [CrossRef]
15. Ananyan, A.A.; Arutyunyan, N.A.; Mazurov, V.A.; Silvestrov, L.K. Permeability of permafrost. In *Permafrost Studies*; MSU Press: Moscow, Russia, 1972; Volume 12, pp. 205–209. (In Russian)
16. Skhalakho, A.S. Conditions of Natural Gas Hydrate Formation in Porous Media and Their Effect on Production Potential of Petroleum Wells. Ph.D. Thesis, The National University of Oil and Gas "Gubkin University", Moscow, Russia, 1974; p. 24. (In Russian).
17. Beznosikov, A.F. Gas Hydrate Deposits and Features of Their Development (Case Study of the Messoyakha Field). Ph.D. Thesis, Industrial University of Tyumen, Tyumen, Russia, 1978; p. 155. (In Russian)
18. Nenakhov, V.A. Infiltration of water through hydrate-saturated porous media. In *EI VNIIEGazprom, Ser. Geol. Buren. Razrab. Gaz. Mestorozhdeniy*; Gazprom VNIIGAZ: Moscow, Russia, 1982; pp. 9–10. (In Russian)
19. Minagawa, H.; Ohmura, R.; Kamata, Y. Water permeability measurements of gas hydrate-bearing sediments. In Proceedings of the Fifth International Conference on Gas Hydrates, Trondheim, Norway, 13–16 June 2005; Tapir Acad. Press: Trondheim, Norway, 2005; pp. 398–401.
20. Johnson, A.; Patil, S.; Dandekar, A. Experimental investigation of gas-water relative permeability for gas-hydrate-bearing sediments from the Mount Elbert Gas Hydrate Stratigraphic Test Well, Alaska North Slope. *Mar. Pet. Geol.* **2011**, *28*, 419–426. [CrossRef]
21. Winters, W.; Walker, W.; Hunter, R.; Collet, T.; Boswell, R.; Rose, K.; Waite, W.; Torres, M.; Patil, S.; Dandekar, A. Physical properties of sediment from the Mount Elbert Gas Hydrate Stratigraphic Test Well, Alaska North Slope. *Mar. Pet. Geol.* **2011**, *28*, 361–380. [CrossRef]
22. Liu, W.; Wu, Z.; Li, Y.; Song, Y.; Ling, Z.; Zhao, J.; Lv, Q. Experimental study on the gas phase permeability of methane hydrate-bearing clayey sediments. *J. Nat. Gas Sci. Eng.* **2016**, *36*, 378–384. [CrossRef]
23. Wu, Z.; Li, Y.; Sun, X.; Li, M.; Jia, R. Experimental study on the gas phase permeability of montmorillonite sediments in the presence of hydrates. *Mar. Pet. Geol.* **2018**, *91*, 373–380. [CrossRef]
24. Wu, Z.; Yang, S.; Liu, W.; Li, Y. Permeability analysis of gas hydrate-bearing sand/clay mixed sediments using effective stress laws. *J. Nat. Gas Sci. Eng.* **2022**, *97*, 104376. [CrossRef]
25. Wu, Z.; Yang, S.; Zhang, L.; Liu, W.; Li, Y. Stress dependence of the gas permeability of montmorillonite sediments in the presence of methane hydrate. *J. Pet. Sci. Eng.* **2022**, *208*, 109697. [CrossRef]
26. Masuda, Y.; Kurihara, M.; Ohuchi, H. A field-scale simulation study on gas productivity of formations containing gas hydrates. In Proceedings of the Fourth International Conference on Gas Hydrates, Yokohama, Japan, 19–23 May 2002; pp. 40–46.
27. Minagawa, H.; Sakamoto, Y.; Komai, T.; Miyazaki, K.; Narita, H. Gas Hydrate: Methane-hydrate-bearing models based on the apparent permeability and apparent pore-size distribution of artificial and natural methane-hydrate-bearing sediment. In Proceedings of the Offshore Technology Conference, Houston, TX, USA, 3–6 May 2010. [CrossRef]
28. Kleinberg, R.L.; Flaum, C.; Griffin, D.D. Deep sea NMR: Methane hydrate growth habit in porous media and its relationship to hydraulic permeability, deposit accumulation, and submarine slope stability. *J. Geophys. Res.* **2003**, *108*, 2508. [CrossRef]
29. Rezaee, R.; Saeedi, A.; Clennell, B. Tight gas sands permeability estimation from mercury injection capillary pressure and nuclear magnetic resonance data. *J. Petrol. Sci. Eng.* **2012**, *88–89*, 92–99. [CrossRef]
30. Hauge, L.P.; Gauteplass, J.; Høyland, M.D. Pore-level hydrate formation mechanisms using realistic rock structures in highpressure silicon micromodels. *Intern. J. Greenh. Gas Control.* **2016**, *53*, 178–186. [CrossRef]
31. Daigle, H. Relative permeability to water or gas in the presence of hydrates in porous media from critical path analysis. *J. Petrol. Sci. Eng.* **2016**, *146*, 526–535. [CrossRef]
32. Shen, P.; Li, X.; Li, Z.; Li, G. Permeability determination of hydrate sediments and a new reduction model considering hydrate growth habit. *Fuel* **2020**, *279*, 118297. [CrossRef]
33. Chuvilin, E.M.; Grebenkin, S.I.; Tkacheva, E.V. Change of gas permeability of gas-saturated sediments during hydrate formation and freezing. In Proceedings of the 8th International Conference on Gas Hydrates, Beijing, China, 28 July–1 August 2014; pp. 1–6.
34. Chuvilin, E.M.; Grebenkin, S.I.; Davletshina, D.A.; Jmaev, M.V. Influence of hydrate formation on gas permeability variations in frozen sands. *Earth's Cryosphere* **2020**, *24*, 40–47. [CrossRef]
35. Chuvilin, E.M.; Grebenkin, S.I.; Zhmaev, M.V. Gas permeability of sandy sediments: Effects of phase changes in pore ice and gas hydrates. *Energy Fuels* **2021**, *35*, 7874–7882. [CrossRef]
36. Chuvilin, E.M.; Grebenkin, S.I. Dissociation of gas hydrates in frozen sands: Effect on gas permeability. *Earth's Cryosphere* **2018**, *22*, 41–45.
37. Chuvilin, E.M.; Grebenkin, S.I.; Pimenov, V.S. Experimental methods for estimation of gas permeability variations in core samples on hydrate saturation and freezing. In Proceedings of the III International Workshop World Gas Resources and Development Perspectives (WGRR 2013), Moscow, Russia, 27–28 November 2013; p. 86.
38. Yershov, E.D. *Methods of Geocryology*; Moscow University Press: Moscow, Russia, 2004; pp. 19–66. (In Russian)

39. Chuvilin, E.; Bukhanov, B.; Davletshina, D.; Grebenkin, S.; Istomin, V. Dissociation and Self-Preservation of Gas Hydrates in Permafrost. *Geosciences* **2018**, *8*, 431. [CrossRef]
40. Istomin, V.A.; Yakushev, V.S.; Makhonina, N.A.; Kwon, V.G.; Chuvilin, E.M. Self-preservation phenomenon of gas hydrate. *Gas Ind. Russ.* **2006**, *4*, 16–27. (In Russian)
41. Chuvilin, E.; Davletshina, D. Formation and Accumulation of Pore Methane Hydrates in Permafrost: Experimental Modeling. *Geosciences* **2018**, *8*, 467. [CrossRef]
42. Chuvilin, E.M.; Guryeva, O.M. Experimental investigation of CO_2 gas hydrate formation in porous media of frozen and freezing sediments. *Earth's Cryosphere* **2009**, *23*, 41–45. (In Russian)